ELSEVIER

Journal of Structural Geology 29 (2007) 435–452

JOURNAL OF STRUCTURAL GEOLOGY

www.elsevier.com/locate/jsg

Numerical modeling of the motion of deformable ellipsoidal objects in slow viscous flows

Dazhi Jiang*

Department of Earth Sciences, University of Western Ontario, London, Ontario, Canada N6A 5B7

Received 15 March 2006; received in revised form 14 September 2006; accepted 22 September 2006
Available online 17 November 2006

Abstract

An algorithm for modeling the strain and rotation of deformable ellipsoidal objects in viscous flows based on Eshelby's (1957. Proceedings of the Royal Society of London A241, 376–396) theory is presented and is implemented in a fully graphic mathematics application (Mathcad®, http://www.mathsoft.com). The algorithm resolves all singular cases encountered in modeling large finite deformations. The orientation of ellipsoidal objects is specified in terms of polar coordinate angles which are easily converted to the trend and plunge angles of the three principal axes rather than the Euler angles. With the Mathcad worksheets presented in the supplementary data associated with this paper, one can model the strain and rotation paths of individual deformable objects and the development of preferred orientation and shape fabrics for a population of deformable objects in any homogeneous viscous flow. The shape and preferred orientation fabrics for a population of deformable objects can be presented in both a three-dimensional form and a two-dimensional form, allowing easy comparison between field data and model predictions. The full graphic interface of Mathcad® makes using the worksheets as easy as using a spreadsheet. The modeler can interact fully with the computation and customize the type and format of the output data to best fit the purpose of the investigation and to facilitate the comparison of model predictions with geological observations.

Keywords: Clast; Rotation; Strain; Fabric development; Numerical modeling; Preferred orientation; Eshelby's theory

1. Introduction

Deformation of the composite material made of one phase (variably called inclusion, object, clast, particle, inhomogeneity, or impurity in the literature) dispersed in another continuous phase (called matrix) has been a subject of research in the broad field of materials science for over a century (Einstein, 1896, 1911, as cited by Jeffery, 1922; Jeffery, 1922; Eshelby, 1957, 1959; Goldsmith and Mason, 1967; Mura, 1987 and references therein). Many rock types in Earth's lithosphere resemble this composite material, such as conglomerates, igneous rocks containing enclaves, xenoliths, or clasts, the melt-crystal mesh at the late stage of magma crystallization, porphyroblast-bearing metamorphic rocks, and porphyroclast-bearing tectonites. A variety of questions have been addressed for the deformation of this composite material including how the presence of inclusions, rigid or deformable, affects the bulk rheological properties of the material (Jeffery, 1922; Goldsmith and Mason, 1967; Treagus, 2002; Treagus and Treagus, 2001, 2002; Fletcher, 2004; Liu and Hu, 2004; Lee and Paul, 2005; Benedikt et al., 2006; Ma et al., 2006), how the motion of an inclusion is related to the bulk deformation kinematics and strain in 3D deformation (Jeffery, 1922; Eshelby, 1957, 1959; Gay, 1968a,b; Bilby et al., 1975; Bilby and Kolbuszewski, 1977; Freeman, 1985, 1987; Passchier and Simpson, 1986; Passchier, 1987) or in 2D deformation (Ghosh and Ramberg, 1976, for rigid, and Bilby and Kolbuszewski, 1977, for deformable elliptical inclusions), and how shape and preferred orientation fabrics evolve with deformation for a population of inclusions (Gay, 1966; Reed and Tryggvason, 1974; Tullis, 1976; Jezek et al., 1994, 1996; Masuda et al., 1995; Launeau and Cruden, 1998; Jiang, in press). There are also many recent works on how

* Tel: +1 519 661 3192; fax: +1 519 661 3198.
E-mail address: djiang3@uwo.ca

0191-8141/$ - see front matter © 2006 Elsevier Ltd. All rights reserved.
doi:10.1016/j.jsg.2006.09.009

the rotational behavior of rigid objects in a viscous flow may be affected by (1) the interface property between the matrix and the object (Ildefonse and Mancktelow, 1993; Mancktelow et al., 2002; Ceriani et al., 2003; Schmid and Podladchikov, 2004, 2005; Mandal et al., 2005b), (2) the boundary constraints where the rigid objects are large compared to the thickness of the hosting shear zone (Marques and Coelho, 2001), (3) the interaction between objects (Ildefonse et al., 1992a,b; Marques and Bose, 2004; Mandal et al., 2005b), and (4) the matrix anisotropy (Mandal et al., 2005a).

This paper is concerned with the motion of deformable inclusions in slow flows. One very special case for the inclusion-bearing material is where the inclusions have identical mechanical properties as the matrix so that the inclusions are passive markers. Ramsay (1967) and Dunnet (1969) have established the relationship between the bulk strain ellipsoid and the shape and orientation fabric defined by passive ellipsoidal inclusions (see also, Lisle, 1985). A second special case is where the inclusions are needle-like or flake-like grains and therefore their behaviors approximate, respectively, material lines and planes to which March's (1932) theory applies (e.g., Tullis, 1976). A third special case is where the inclusions are small rigid ellipsoidal objects to which Jeffery's (1922) theory applies. Jeffery's (1922) theory has been extended to more general cases by Bretherton (1962) and Willis (1977) and has been tested by many experiments (Taylor, 1923; Eirich and Mark, 1937; Trevelyan and Mason, 1951; Goldsmith and Mason, 1967; Robertson and Acrivos, 1970; Ghosh and Ramberg, 1976; ten Brink, 1996; Arbaret et al., 2001). Beyond the above special cases, the general situation is where the inclusions are deformable and exhibit a competence contrast with respect to the surrounding matrix. Eshelby (1957, 1959) develops the theory for the motion of deformable ellipsoidal inclusions embedded in a continuous matrix. The original theory (Eshelby, 1957, 1959) was formulated for the case where both the inclusion and the matrix are isotropic and linearly elastic. It has been extended to the case where both the inclusion and the surrounding matrix are linear viscous fluids with different viscosities (Bilby et al., 1975; Bilby and Kolbuszewski, 1977). To the motion of a deformable inclusion embedded in a slow viscous flow, Eshelby's theory is what Jeffery's theory is to the motion of a rigid inclusion embedded in a slow viscous flow.

Compared to Jeffery's theory, Eshelby's theory is inevitably more complex. Because a rigid object does not change shape, its orientation completely defines its instantaneous state which amounts to three variables: either the three Euler angles (Jeffery, 1922; Bretherton, 1962; Freeman, 1985) or the three polar coordinate angles used by Jiang (in press) which in general are equivalent to the trend and plunge of one principal axis plus the trend of a second principal axis. For a deformable object, its instantaneous state must be defined by its orientation (three variables), competence contrast relative to the matrix (one variable), as well as the instantaneous lengths of the three principal axes (three variables). Altogether, seven variables are required to define an instantaneous state of a deformable ellipsoidal object. This makes Eshelby's theory more complex than Jeffery's. The associated equations are also more challenging and computationally more intensive to solve. So far, Freeman (1987) has only made attempt on the numerical solution of Eshelby's equations in comparison with many numerical solutions to Jeffery's equations (see Jiang, in press and references therein).

The purpose of this paper is to achieve, for modeling the motion of deformable inclusions based on Eshelby's (1957, 1959) theory, what Jiang (in press) has achieved for modeling the motion of rigid inclusions based on Jeffery's (1922) theory. Specifically, I develop an algorithm for solving Eshelby's equations and implement it in a fully graphic mathematics application, Mathcad® (http://www.mathsoft.com), so that the modeling is as simple and user-friendly as using a spreadsheet. Examples of application are presented in the paper for many cases to demonstrate the robustness of the worksheets. However, the focus of the paper is on the algorithm and its implementation, not on a systematic investigation of the behavior of deformable inclusions in viscous flows.

2. Summary of Eshelby's theory

Eshelby (1957, 1959) considers the elastic field inside and outside an ellipsoidal inclusion embedded in an infinite elastic body. Both the inclusion and the encompassing matrix are isotropic and linearly elastic but may have different elastic constants. Although the elastic field in the vicinity outside the inclusion is heterogeneous (Eshelby, 1959), Eshelby (1957) discovered, remarkably, that within the inclusion the elastic field is perfectly homogeneous as long as the inclusion is ellipsoidal. By the well-known equivalence between the theory of linear elasticity and the theory of Newtonian fluids, Eshelby's theory is readily formulated for the case where both the inclusion and the encompassing matrix are Newtonian fluids but with, in general, different viscosities (Bilby et al., 1975). I summarize Eshelby's theory below, starting with some necessary background on the mathematical description of the kinematics of motion in different reference frames and their associated coordinate systems.

2.1. Flow described in different reference frames and the rotation of one reference frame with respect to another

Let us denote the instantaneous lengths of the three principal semi-axes of the ellipsoidal inclusion a_1, a_2, and a_3 and consider two reference frames. One is the reference frame, R', *always* parallel to the principal axes of the ellipsoidal inclusion. The right-handed Cartesian coordinate system associated with R' is $x_1'x_2'x_3'$, with x_i'-axes parallel to the corresponding a_i-axes ($i = 1-3$, Fig. 1). Another reference frame is the fixed external frame, R, in which the flow of the matrix fluid is defined and the Cartesian coordinate system associated with it is $x_1x_2x_3$ (Fig. 1). We now describe the matrix flow in each of the two reference frames and state the rotation of R' with respect to R mathematically.

In this paper, the following general scheme of mathematical notation is used. Scalars are in lowercase italics (such as a_1, a_2, a_3 for the three semi-axial lengths of the inclusion), vectors are in lowercase bold faces, and tensors are in uppercase bold

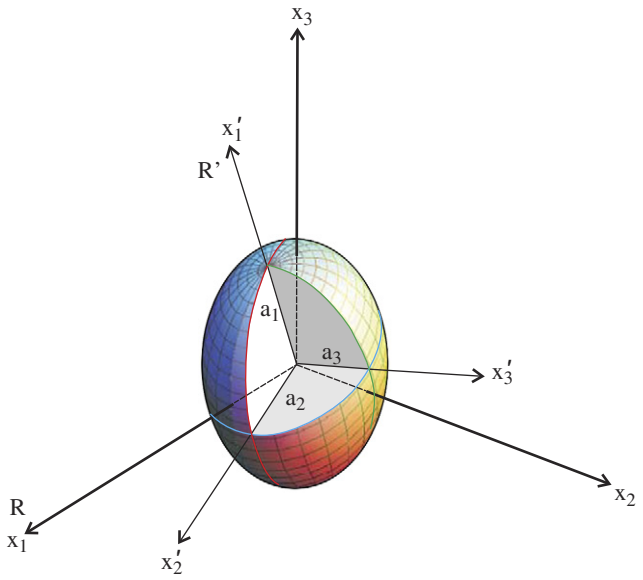

Fig. 1. Two reference frames R and R' and their associated Cartesian coordinate systems. R is the fixed external reference frame and its associated coordinate system is $x_1x_2x_3$. The flow of the matrix is defined in this frame and coordinate system. R' is *always* parallel to the three principal axes of the ellipsoidal inclusion. The associated coordinate system is $x_1'x_2'x_3'$. The instantaneous three semi-axes of the inclusion are a_1, a_2, and a_3 which can have any relative lengths.

faces. A bold face letter without a prime sign stands for a vector or tensor defined in the R frame *and* expressed in x_i-coordinates (e.g., $\mathbf{W}$ stands for vorticity with respect to R and its components, W_{ij}, are stated in terms of x_i-coordinates). A bold face letter with a prime sign stands for a vector or tensor defined in the R' frame *and* expressed in x'_i-coordinates (e.g. $\mathbf{W}'$ stands for vorticity with respect to R' and its components, W'_{ij}, are in terms of x'_i-coordinates). A bold face uppercase letter with a wave bar (e.g., $\tilde{\mathbf{W}}$) stands for a tensor defined with respect to R but is expressed in x_i' coordinates. This scheme of notation is followed as far as possible in this paper; wherever a new notation is used its meaning is fully explained.

Suppose the base unit vectors parallel to the x_i' are $\mathbf{e}_i'$ ($i = 1, 2, 3$ throughout the paper) which are all functions of time because R' rotates continuously with respect to R. The base unit vectors parallel to x_i are $\mathbf{e}_i$. A position vector in space can be expressed either in terms of base vectors $\mathbf{e}_i$ or base vectors $\mathbf{e}_i'$. In the former case the vector is denoted $\mathbf{x}$ with x_i coordinates and in the latter case it is denoted $\mathbf{x}'$ with x_i' coordinates. The components of $\mathbf{x}$ and $\mathbf{x}'$ are related by (e.g., Spencer, 1980, pp.64–66):

$$\mathbf{x}' = \mathbf{Q}\mathbf{x} \tag{1a}$$

$$\mathbf{x} = \mathbf{Q}^{\mathrm{T}}\mathbf{x}' \tag{1b}$$

where $\mathbf{Q}$ is the transformation tensor ($\mathbf{Q}^{\mathrm{T}}$, its transpose) of coordinates from x_i to x_i' defined by:

$$\mathbf{e}_i' = \mathbf{Q}\mathbf{e}_i \tag{2a}$$

$$\mathbf{e}_i = \mathbf{Q}^{\mathrm{T}}\mathbf{e}_i' \tag{2b}$$

Being an orthogonal tensor, $\mathbf{Q}$ has the following property (e.g. Başar and Weichert, 2000, p. 29):

$$\mathbf{Q}\mathbf{Q}^{\mathrm{T}} = \mathbf{Q}^{\mathrm{T}}\mathbf{Q} = \mathbf{I} \tag{3}$$

where $\mathbf{I}$ is a unit tensor ($I_{ij} = 0$ if $i \neq j$, $I_{ij} = 1$ if $i = j$).

The homogeneous matrix flow is described in R by its Eulerian velocity gradient tensor $\mathbf{L}$:

$$\mathbf{v} = \frac{\mathrm{d}\mathbf{x}}{\mathrm{d}t} = \mathbf{L}\mathbf{x} \tag{4}$$

where $\mathbf{v}$ is the particle velocity vector field as observed in R ($\mathbf{v}'$ below is the particle velocity vector field as observed in R').

To find out the expression of the velocity gradient of the matrix flow in R', we differentiate Eq. (1a) with respect to time and make use of Eq. (1b) as well as Eq. (4), leading to:

$$\mathbf{v}' = \frac{\mathrm{d}\mathbf{x}'}{\mathrm{d}t} = \dot{\mathbf{Q}}\mathbf{x} + \mathbf{Q}\frac{\mathrm{d}\mathbf{x}}{\mathrm{d}t} = \left(\dot{\mathbf{Q}}\mathbf{Q}^{\mathrm{T}} + \mathbf{Q}\mathbf{L}\mathbf{Q}^{\mathrm{T}}\right)\mathbf{x}' \tag{5}$$

where the dot on top of $\mathbf{Q}$ stands for its derivative with respect to time. From Eq. (5), the velocity gradient tensor $\mathbf{L}'$ in R' is:

$$\mathbf{L}' = \dot{\mathbf{Q}}\mathbf{Q}^{\mathrm{T}} + \mathbf{Q}\mathbf{L}\mathbf{Q}^{\mathrm{T}} \tag{6}$$

The velocity gradient tensors, $\mathbf{L}$ and $\mathbf{L}'$, can be decomposed into their corresponding symmetric strain rate tensors and antisymmetric vorticity tensors (e.g., Spencer, 1980) according to:

$$\mathbf{D} = \frac{1}{2}\left(\mathbf{L} + \mathbf{L}^{\mathrm{T}}\right), \quad \mathbf{W} = \frac{1}{2}\left(\mathbf{L} - \mathbf{L}^{\mathrm{T}}\right) \tag{7a}$$

$$\mathbf{D}' = \frac{1}{2}\left(\mathbf{L}' + \mathbf{L}'^{\mathrm{T}}\right), \quad \mathbf{W}' = \frac{1}{2}\left(\mathbf{L}' - \mathbf{L}'^{\mathrm{T}}\right) \tag{7b}$$

Applying this decomposition to Eq. (6) and making use of the identity $\dot{\mathbf{Q}}\mathbf{Q}^{\mathrm{T}} = -\mathbf{Q}\dot{\mathbf{Q}}^{\mathrm{T}}$, which can be obtained by differentiating Eq. (3) with respect to time, leads to:

$$\mathbf{D}' = \mathbf{Q}\mathbf{D}\mathbf{Q}^{\mathrm{T}} \tag{8a}$$

$$\mathbf{W}' = \mathbf{Q}\mathbf{W}\mathbf{Q}^{\mathrm{T}} + \dot{\mathbf{Q}}\mathbf{Q}^{\mathrm{T}} = \tilde{\mathbf{W}} + \dot{\mathbf{Q}}\mathbf{Q}^{\mathrm{T}} \tag{8b}$$

Eq. (8) is the mathematical expression of the Zorawski theorem (Truesdell and Topin, 1960, p. 440) which states: "For a given flow, observers in two rigid frames moving arbitrarily with respect to one another perceive the same stretching (i.e., strain rate), but vorticities which differ by the relative angular velocity of the frames". To further explain the physical significance of the terms in Eq. (8b), let us write the vorticity transformation between frames in a form similar to that used by Lister (1982) and Lister and Williams (1983):

$$\mathbf{W}^{R'} = \mathbf{W}^{R} + \mathbf{W}_{R}^{R'} \tag{9}$$

Eq. (9) states that the vorticity with respect to frame R', $\mathbf{W}^{R'}$, is equal to the vorticity with respect to frame R, $\mathbf{W}^{R}$, plus the vorticity appropriate for the angular velocity of frame R with respect to frame R', $\mathbf{W}_{R}^{R'}$. Comparing Eq. (8b) with Eq. (9),

$\mathbf{W}' = \mathbf{W}^{R'}$, and $\tilde{\mathbf{W}}$ is the vorticity with respect to R (i.e., $\mathbf{W}^R = \tilde{\mathbf{W}}$) expressed in the same coordinates as $\mathbf{W}'$. It is therefore clear that the term $\mathbf{Q}\cdot\mathbf{Q}^{\mathrm{T}}$ in Eq. (8b) is equal to $\mathbf{W}_R^{R'}$, representing the angular velocity of frame R with respect to frame R'. Our interest is the angular velocity of R' with respect to R. Since $\mathbf{W}_R^{R'} + \mathbf{W}_{R'}^{R} \equiv 0$, we have:

$$\mathbf{W}_{R'}^{R} = -\mathbf{W}_R^{R'} = -\dot{\mathbf{Q}}\mathbf{Q}^{\mathrm{T}} \tag{10}$$

Eq. (10) is the tensor describing the instantaneous rotation of the principal axes of the inclusion (R') with respect to the fixed reference frame (R). We denote this tensor $\tilde{\mathbf{\Theta}}$ hereafter:

$$\tilde{\mathbf{\Theta}} = -\dot{\mathbf{Q}}\mathbf{Q}^{\mathrm{T}} \tag{11}$$

If stated in the x_i coordinates, it is:

$$\mathbf{\Theta} = \mathbf{Q}^{\mathrm{T}}\tilde{\mathbf{\Theta}}\mathbf{Q} \tag{12}$$

Since $\mathbf{\Theta}$ describes the instantaneous angular velocity of the inclusion, to determine the rotation of the inclusion principal axes with respect to R is to determine the time history of $\mathbf{\Theta}$.

2.2. Flow within the ellipsoidal inclusion

Within the ellipsoidal inclusion, the flow is homogeneous but differs from the matrix flow. Eshelby (1957, 1959) and Bilby et al. (1975) show that the vorticity and strain rate tensors for the flow within the inclusion, measured in R' and expressed in x_i' coordinates, are:

$$W_{ij}^{\mathrm{E}} = W_{ij}' + (1-r)\Pi_{ijkl}D_{kl}^{\mathrm{E}} \tag{13a}$$

$$D_{ij}^{\mathrm{E}} = D_{ij}' + (1-r)S_{ijkl}D_{kl}^{\mathrm{E}} \tag{13b}$$

where S_{ijkl} and Π_{ijkl} are called Eshelby tensors (Mura, 1987; Lee and Paul, 2005) that relate the flow inside the ellipsoid with the flow of the matrix fluid, the superscript E stands for the ellipsoidal inclusion, and r is the viscosity ratio of the ellipsoid to the matrix. The repeated subscript in Eq. (13) is taken to imply summation over the values 1, 2, and 3 of that subscript. This summation convention is used throughout the paper unless a 'no summation' is declared locally.

The non-zero components of the two Eshelby's tensors, expressed in the x'_i coordinates, are (Eshelby, 1957):

$$\begin{aligned}
S_{iiii} &= \frac{3}{4\pi}a_i^2 J_{ii},\\
S_{iijj} &= \frac{3}{4\pi}a_j^2 J_{ij},\\
S_{ijij} &= \frac{3}{8\pi}\left(a_i^2 + a_j^2\right)J_{ij}\\
\Pi_{ijij} &= \Pi_{ijji} = \frac{J_j - J_i}{8\pi},\\
\Pi_{jiij} &= \Pi_{jiji} = -\Pi_{ijij} \qquad \text{no summation}
\end{aligned} \tag{14}$$

In Eq. (14), the J-terms are defined as follows (Jeffery, 1922; Eshelby, 1957):

$$\begin{aligned}
J_i &= 2\pi a_1 a_2 a_3 \int_0^\infty \frac{\mathrm{d}u}{(a_i^2+u)\lambda} \quad (i=1,2,3)\\
J_{ii} &= 2\pi a_1 a_2 a_3 \int_0^\infty \frac{\mathrm{d}u}{(a_i^2+u)^2\lambda} \quad (i=1,2,3)\\
J_{ij} &= 2\pi a_1 a_2 a_3 \int_0^\infty \frac{\mathrm{d}u}{(a_i^2+u)(a_j^2+u)\lambda} \quad (i=1,2,3;\\
&\qquad\qquad\qquad\qquad\qquad\qquad j=1,2,3;\ i\neq j)
\end{aligned} \tag{15}$$

In the above equalities, $\lambda = \sqrt{(a_1^2+u)(a_2^2+u)(a_3^2+u)}$.

Mura (1987, pp. 79–84) gives the J-integrals in elementary functions for all possible shapes of inclusions. This is only useful in branches of materials science where the strain is small and deformation history of the inclusion is simple (e.g., Lee and Paul, 2005). In the process of a progressive deformation to large finite strains commonly encountered in geology, the shape of an inclusion may change from one special shape to another (e.g., from a triaxial ellipsoid to a spheroid) and it is also possible for the relative lengths of the principal axes of an inclusion to change during deformation. It is not possible to use the elementary function forms of Mura (1987) for the J-terms; they must be in general evaluated from the integrals of Eq. (15).

Eq. (13b) can be expanded to give the following equalities for the strain rate tensor components of the ellipsoidal inclusion (Freeman, 1987)[1]:

$$\begin{aligned}
D_{11}^{\mathrm{E}} &= \frac{D_{11}'[1+(r-1)(S_{2222}-S_{2233})] + D_{22}'[(r-1)(S_{1133}-S_{1122})]}{K}\\
D_{22}^{\mathrm{E}} &= \frac{D_{11}'[(r-1)(S_{2233}-S_{2211})] + D_{22}'[1+(r-1)(S_{1111}-S_{1133})]}{K}\\
D_{33}^{\mathrm{E}} &= -\left(D_{11}^{\mathrm{E}} + D_{22}^{\mathrm{E}}\right),\ D_{12}^{\mathrm{E}} = \frac{D_{12}'}{1+2(r-1)S_{1212}},\\
D_{13}^{\mathrm{E}} &= \frac{D_{13}'}{1+2(r-1)S_{1313}},\ D_{23}^{\mathrm{E}} = \frac{D_{23}'}{1+2(r-1)S_{2323}}
\end{aligned} \tag{16}$$

In the above equalities, K is defined as

$$\begin{aligned}
K = 1 &+ (r-1)(S_{1111} + S_{2222} - S_{2233} - S_{1133})\\
&+ (r-1)^2[S_{1111}(S_{2222} - S_{2233}) + S_{1133}(S_{2211} - S_{2222})\\
&+ S_{1122}(S_{2233} - S_{2211})]
\end{aligned}$$

To find out the components of W_{ij}^{E}, we proceed with the following. To ensure that the x_i'-axes *always* do coincide with the

[1] The expansion of Eq. (13b) presented in Freeman (1987) contains some errors/typos.

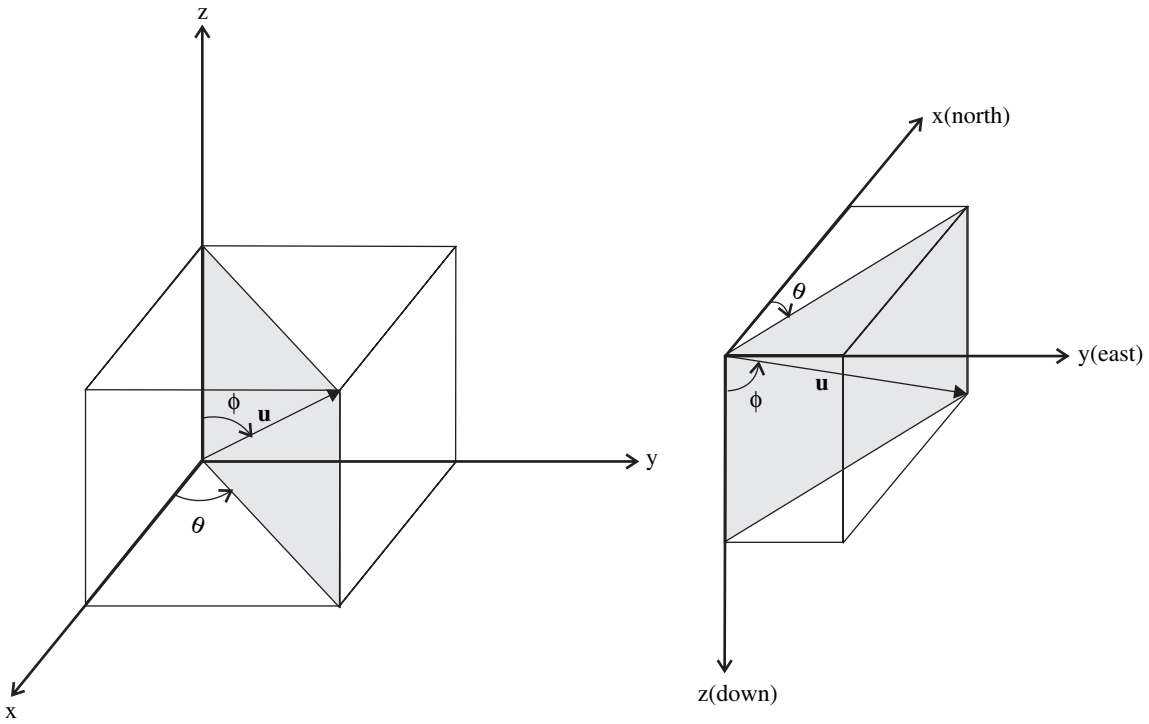

Fig. 2. (a) The orientation of a line in 3D space can be represented by a unit vector, **u**, with two coordinate angles: θ, the angle between the projection of **u** in xy plane with the x-axis and ϕ the angle between **u** and the z-axis. (b) If xyz is the geographic coordinate system and $\phi < 90^\circ$, then θ is the plunge direction of **u** and ϕ is the complementary angle of the plunge of **u** (i.e., the plunge angle $= 90^\circ - \phi$). If xyz is the geographic coordinate system and $\phi > 90^\circ$, then $\theta \pm 90^\circ$ is the plunge direction of **u** and $\phi - 90^\circ$ is the plunge angle of **u**.

principal axes of the ellipsoid, we follow Goddard and Miller (1967) and Bilby and Kolbuszewski (1977) by defining the instantaneous ellipsoid surface by the following equation:

$$G_{ij}x_i'x_j' = 1 \tag{17}$$

where G_{ij} is the ellipsoid tensor for the instantaneous inclusion surface. We require that G_{ij} be diagonal with the components $G_{ii} = 1/a_i^2$ for $i = j$ and $G_{ij} = 0$ for $i \neq j$. This ensures that the x_i'-axes are always parallel to the principal axes of the ellipsoid. Differentiating Eq. (17) with respect to time and using the symmetry of G_{ij} and the fact that within the ellipsoid and on its surface, $(\mathrm{d}x_i'/\mathrm{d}t) = (D_{ij}^{\mathrm{E}} + W_{ij}^{\mathrm{E}})x_j'$, we obtain (Eq. (4); Bilby and Kolbuszewski, 1977):

$$\frac{\mathrm{d}G_{ij}}{\mathrm{d}t} + G_{is}\left(D_{sj}^{\mathrm{E}} + W_{sj}^{\mathrm{E}}\right) + G_{js}\left(D_{si}^{\mathrm{E}} + W_{si}^{\mathrm{E}}\right) = 0 \tag{18}$$

The above equation leads to:

$$\frac{\mathrm{d}G_{ij}}{\mathrm{d}t} + \left(G_{ii} + G_{jj}\right)D_{ij}^{\mathrm{E}} + \left(G_{ii} - G_{jj}\right)W_{ij}^{\mathrm{E}} = 0 \quad \text{no summation} \tag{19}$$

This equation is examined for two different situations below.

2.2.1. The situation the inclusion is a triaxial ellipsoid

For a triaxial ellipsoid, $a_i \neq a_j$ (equivalent to $G_{ii} \neq G_{jj}$) and Eq. (19) gives the following relations for the vorticity of the flow inside the inclusion and the instantaneous strain rates along the principal axes of the ellipsoid:

$$W_{ij}^{\mathrm{E}} = \frac{a_i^2 + a_j^2}{a_i^2 - a_j^2}D_{ij}^{\mathrm{E}}, \quad \text{if} a_i \neq a_j \quad \text{no summation} \tag{20}$$

$$\frac{\mathrm{d}a_i}{\mathrm{d}t} = a_i D_{ii}^{\mathrm{E}} \quad (i = 1,2,3) \quad \text{no summation} \tag{21}$$

Combining Eqs. (8b), (11), (13a), and (20), we have for a triaxial ellipsoid:

$$\tilde{\Theta}_{ij} = \tilde{W}_{ij} - (r-1)\Pi_{ijkl}D_{kl}^{\mathrm{E}} - \frac{a_i^2 + a_j^2}{a_i^2 - a_j^2}D_{ij}^{\mathrm{E}} \quad \text{summation over } k\,(=1,2,3) \text{ and } l\,(=1,2,3) \text{ only} \tag{22}$$

The three independent non-zero components of $\tilde{\mathbf{\Theta}}$ are then:

$$\tilde{\Theta}_{12} = \tilde{W}_{12} - 2(r-1)\Pi_{1212}D_{12}^{\mathrm{E}} - \frac{a_1^2 + a_2^2}{a_1^2 - a_2^2}D_{12}^{\mathrm{E}} \quad (a_1 \neq a_2)$$

$$\tilde{\Theta}_{13} = \tilde{W}_{13} - 2(r-1)\Pi_{1313}D_{13}^{\mathrm{E}} - \frac{a_1^2 + a_3^2}{a_1^2 - a_3^2}D_{13}^{\mathrm{E}} \quad (a_1 \neq a_3)$$

$$\tilde{\Theta}_{32} = \tilde{W}_{32} - 2(r-1)\Pi_{3232}D_{23}^{\mathrm{E}} - \frac{a_3^2 + a_2^2}{a_3^2 - a_2^2}D_{23}^{\mathrm{E}} \quad (a_2 \neq a_3) \tag{23}$$

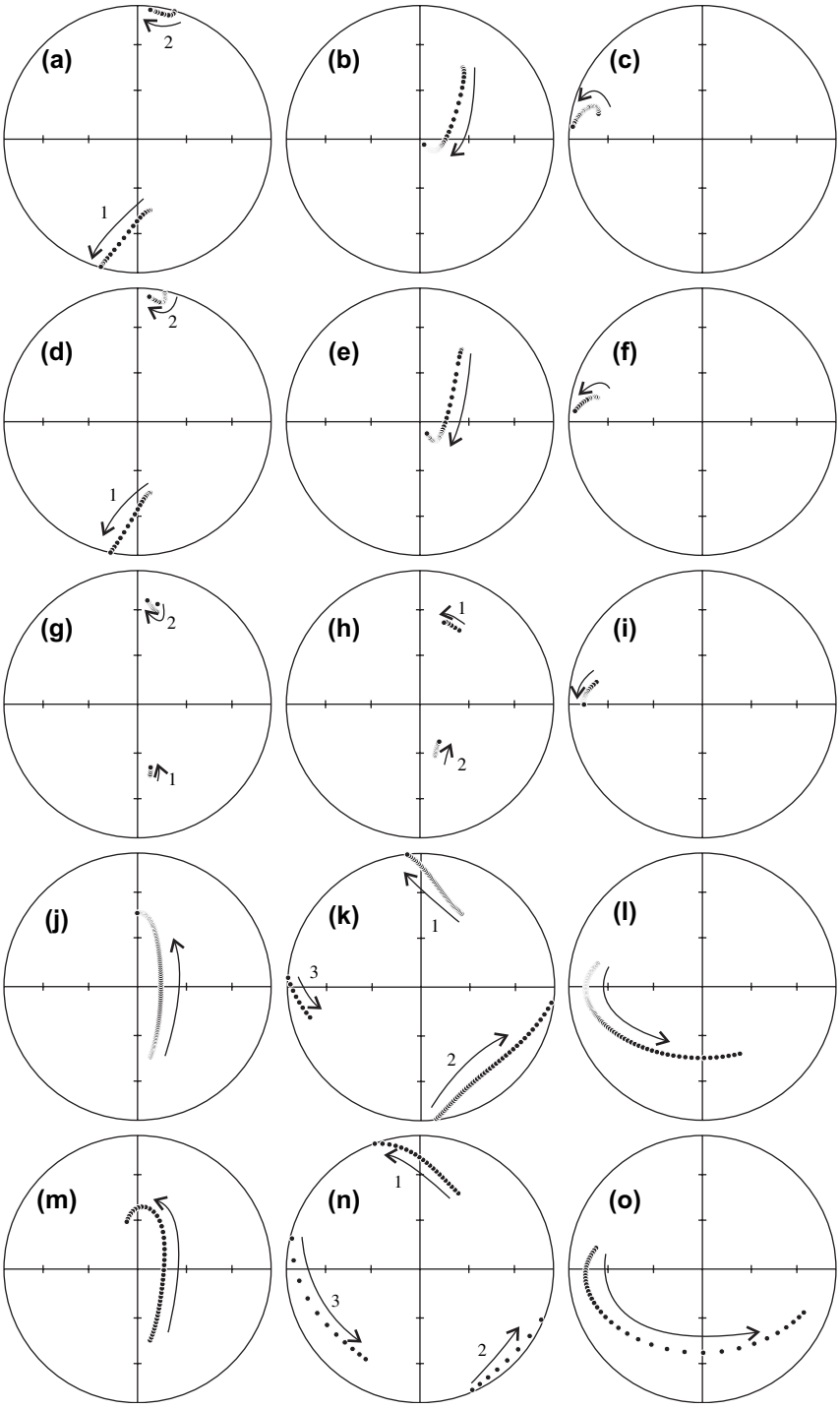

Fig. 3. Rotation paths of a triaxial inclusion with initial axial length ratios of 5:3:1 and initial orientation of (170°, 45°, 30°) in simple shear for various viscosity ratios (numerical experiment set 1). The final shear strain is 10. (a–c) The paths, respectively, for a_1, a_2, and a_3 axes for viscosity ratio of 0.1. (d–f) The paths for viscosity ratio of 1. (g–i) The paths for viscosity ratio of 5. (j–l) The paths for viscosity ratio of 20. (m, n, o) The paths for a rigid inclusion (5:3:1) with the same initial orientation modeled using Mathcad worksheet of Jiang (in press). Arrows in each plot indicate the strain increase direction and numbers indicate the order of the rotation paths. In this and all subsequent figures, the geographic coordinate system (Fig. 2b) is used. The flow is a simple shear with the shear direction parallel to the x-axis, and the sense of shear is sinistral.

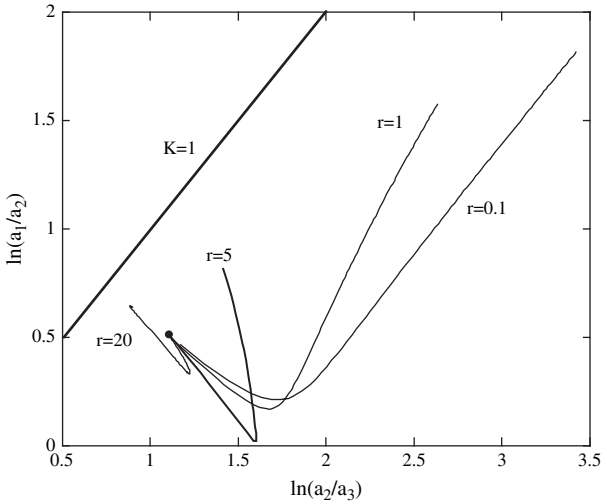

Fig. 4. The paths for the shape change of the inclusion in numerical experiment set 1 presented in a logarithm Flinn plot.

2.2.2. Singular cases where the inclusion is a spheroid or sphere

In the event that the ellipsoid is spheroidal ($a_i = a_j$, equivalent to $G_{ii} = G_{jj}$) (either so shaped initially or the inclusion passes through this shape at some instant in its course of deformation), Eq. (20) is singular and the angular velocity of the principal axes of the object is undefined. We note that in this case Eq. (19) becomes

$$\frac{\mathrm{d}G_{ij}}{\mathrm{d}t} + 2G_{ii}D^{\mathrm{E}}_{ij} = 0 \quad (i \neq j) \quad \text{no summation} \tag{24}$$

Unless $D^{\mathrm{E}}_{ij} = 0$, the above equation cannot hold under the condition of $G_{ij} = 0$ ($i \neq j$) which is required to ensure that the x'_i axes are always the principal axes of the ellipsoid (Goddard and Miller, 1967). To ensure that $D^{\mathrm{E}}_{ij} = 0$, the x'_i- and x'_j-axes on the circular $a_i a_j$-section of the ellipsoid must be exactly parallel to the principal directions of the flow of the ellipsoid on that section. By examining Eq. (16), it can be seen that D^{E}_{ij} vanishes

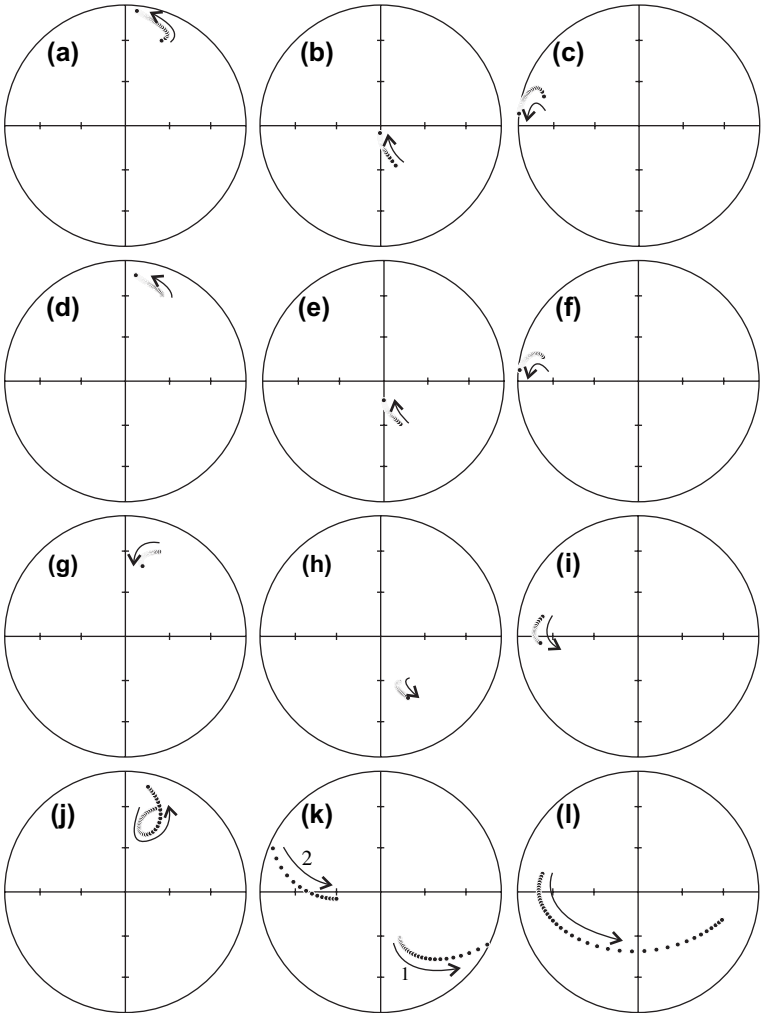

Fig. 5. Rotation paths of an initially oblate inclusion with axial length ratios of 5:5:2 and initial orientation of (170°, 45°, 30°) in simple shear for various viscosity ratios (numerical experiment set 2). The matrix final shear strain is 10. (a–c) The paths, respectively, for a_1, a_2, and a_3 axes for viscosity ratio of 0.1. (d–f) The paths for viscosity ratio of 1. (g–i) The paths for viscosity ratio of 5. (j–l) The paths for viscosity ratio of 20.

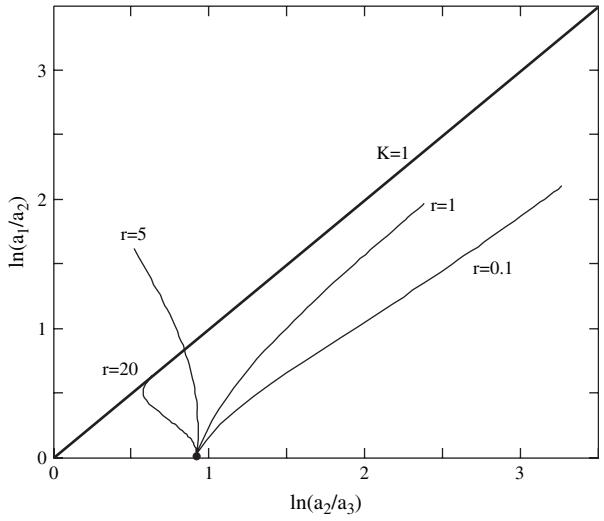

Fig. 6. The paths for the shape change of the inclusion in numerical experiment set 2 presented in a logarithm Flinn plot.

when D'_{ij} vanishes. That is the principal directions of $\mathbf{D}^{\mathrm{E}}$ coincide with those of $\mathbf{D}'$. Therefore at the instant $a_i = a_j$, instead of letting $\tilde{\Theta}_{ij}$, which is not definable when $a_i = a_j$, decide the rotation of $\mathbf{e}'_i$ and $\mathbf{e}'_j$, we can perform a rotation on them around $\mathbf{e}'_k$ axis until they are parallel, respectively, to the two principal directions of the sectional flow on the a_ia_j-plane at that instant so that Eq. (24) is satisfied. To do so, we first find the principal directions of the sectional flow on the a_ia_j-plane ($a_i = a_j \neq a_k$) by taking the eigenvectors of the 2D submatrix of $\mathbf{D}'$, that is

$$\mathbf{D}^{\text{plane } ij} = \begin{pmatrix} D'_{ii} & D'_{ij} \\ D'_{ij} & D'_{jj} \end{pmatrix} \tag{25}$$

The direction of the maximum principal rate of $\mathbf{D}^{\text{plane } ij}$ makes an angle ϖ_{ij} with respect to the current $\mathbf{e}'_i$-axis defined by:

$$\varpi_{ij} = \tan^{-1}\left(\frac{D'_{jj} - D'_{ii} + \sqrt{\left(D'_{ii} - D'_{jj}\right)^2 + 4D'^2_{ij}}}{2D'_{ij}}\right) \quad \text{no summation} \tag{26}$$

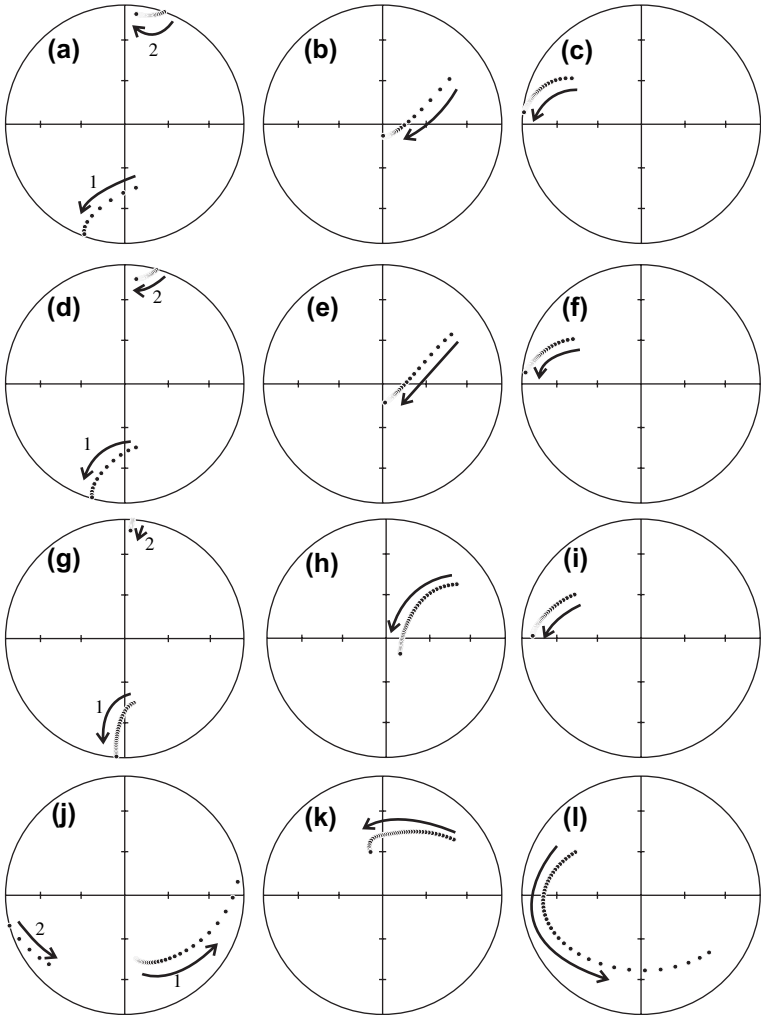

Fig. 7. Rotation paths of an initially prolate inclusion with axial length ratios of 5:2:2 and initial orientation of (170°, 45°, 30°) in simple shear for various viscosity ratios (numerical experiment set 3). The matrix final shear strain is 10. (a–c) The paths respectively for a_1, a_2, and a_3 axes for viscosity ratio of 0.1. (d–f) The paths for viscosity ratio of 1. (g–i) The paths for viscosity ratio of 5. (j–l) The paths for viscosity ratio of 20.

We now rotate the existing $\mathbf{e}'_i(t_n)$ and $\mathbf{e}'_j(t_n)$ axes around the $\mathbf{e}'_k(t_n)$-axis by the angular amount of ϖ_{ij}. Since this is a finite rotation, the axes after rotation are, respectively (Spencer, 1980, pp. 64–66; Başar and Weichert, 2000, pp. 29–33):

$$\begin{aligned}
&\mathbf{e}'^{*}_k(t_n) = \mathbf{e}'_k(t_n)\\
&\mathbf{e}'^{*}_i(t_n) = \cos\varpi_{ij}\mathbf{e}'_i(t_n) + \sin\varpi_{ij}\mathbf{e}'_j(t_n) \quad (i\neq j\neq k) \text{ and no summation}\\
&\mathbf{e}'^{*}_j(t_n) = -\sin\varpi_{ij}\mathbf{e}'_i(t_n) + \cos\varpi_{ij}\mathbf{e}'_j(t_n)
\end{aligned} \tag{27}$$

To disable the effect of the ij-component of $\tilde{\mathbf{\Theta}}$ ($\tilde{\Theta}_{ij} = -\tilde{\Theta}_{ji}$), which is not definable, set $\tilde{\Theta}_{ij} = -\tilde{\Theta}_{ji} = 0$. We thus can extend Eq. (23) to include the singular case where the inclusion is a spheroid:

$$\begin{aligned}
\tilde{\Theta}_{12} &= \begin{cases} 0 & \text{if } a_1 = a_2 \\ \tilde{W}_{12} - 2(r-1)\Pi_{1212}D^E_{12} - \dfrac{a_1^2+a_2^2}{a_1^2-a_2^2}D^E_{12} & \text{otherwise} \end{cases}\\
\tilde{\Theta}_{13} &= \begin{cases} 0 & \text{if } a_1 = a_3 \\ \tilde{W}_{13} - 2(r-1)\Pi_{1313}D^E_{13} - \dfrac{a_1^2+a_3^2}{a_1^2-a_3^2}D^E_{13} & \text{otherwise} \end{cases}\\
\tilde{\Theta}_{32} &= \begin{cases} 0 & \text{if } a_2 = a_3 \\ \tilde{W}_{32} - 2(r-1)\Pi_{3232}D^E_{23} - \dfrac{a_3^2+a_2^2}{a_3^2-a_2^2}D^E_{23} & \text{otherwise} \end{cases}
\end{aligned} \tag{28}$$

The rotation tensor in the x_i coordinates, $\mathbf{\Theta}$, is obtained from Eq. (28) by using Eq. (12).

By the same argument, in the event the inclusion is instantaneously a sphere (and every component of $\mathbf{\Theta}$ is zero according to Eq. (28)), $\mathbf{e}'_i(t_{n+1})$ are set to be parallel to the three principal directions of $\mathbf{D}^{\mathrm{E}}$. Since the principal directions of $\mathbf{D}^{\mathrm{E}}$ and $\mathbf{D}$ coincide in this case, we simply take the eigenvectors of $\mathbf{D}$ and assign them as the new directions for the instantaneous state the inclusion is a perfect sphere, that is,

$$\mathbf{e}'_i(t_{n+1}) = \text{eigenvectors of } \mathbf{D}, \quad \text{if object is sphere at } t_n \quad (i=1,2,3) \tag{29}$$

2.3. Rotation and strain of the ellipsoidal inclusion

The rotation of the principal axes of the ellipsoid is described by the time rate of $\mathbf{e}'_i$ (Eq. (6) of Jiang, 1999). The rotation and shape change of the ellipsoid are completely described by:

$$\frac{\mathrm{d}\mathbf{e}'_i}{\mathrm{d}t} = \mathbf{\Theta}\mathbf{e}'_i \ (i=1,2,3) \tag{30a}$$

$$\frac{\mathrm{d}a_i}{\mathrm{d}t} = a_i D^{\mathrm{E}}_{ii} \ (i=1,2,3) \quad \text{no summation} \tag{30b}$$

Eqs. (30a) and (30b) in general can only be solved numerically. To do so, we use the Runge–Kutta fourth-order method (e.g., Jeffrey, 1995, pp. 340–341) which for Eq. (30a) leads to:

$$\begin{aligned}
&k_1 = \delta t\mathbf{\Theta}(t_n)\mathbf{e}'_i(t_n)\\
&k_2 = \delta t\mathbf{\Theta}\left(t_n+\frac{\delta t}{2}\right)\left(\mathbf{e}'_i(t_n)+\frac{1}{2}k_1\right)\\
&k_3 = \delta t\mathbf{\Theta}\left(t_n+\frac{\delta t}{2}\right)\left(\mathbf{e}'_i(t_n)+\frac{1}{2}k_2\right) \quad \text{for a triaxial inclusion}\\
&k_4 = \delta t\mathbf{\Theta}(t_n+\delta t)(\mathbf{e}'_i(t_n)+k_3)\\
&\mathbf{e}'_i(t_{n+1}) \approx \mathbf{e}'_i(t_n) + \frac{1}{6}(k_1+2k_2+2k_3+k_4) \ (i=1,2,3)
\end{aligned} \tag{31a}$$

$$\begin{aligned}
&k_1 = \delta t\mathbf{\Theta}(t_n)\mathbf{e}'^{*}_i(t_n)\\
&k_2 = \delta t\mathbf{\Theta}\left(t_n+\frac{\delta t}{2}\right)\left(\mathbf{e}'^{*}_i(t_n)+\frac{1}{2}k_1\right)\\
&k_3 = \delta t\mathbf{\Theta}\left(t_n+\frac{\delta t}{2}\right)\left(\mathbf{e}'^{*}_i(t_n)+\frac{1}{2}k_2\right) \quad \text{for a spheroid}\\
&k_4 = \delta t\mathbf{\Theta}(t_n+\delta t)(\mathbf{e}'^{*}_i(t_n)+k_3)\\
&\mathbf{e}'_i(t_{n+1}) \approx \mathbf{e}'^{*}_i(t_n) + \frac{1}{6}(k_1+2k_2+2k_3+k_4) \quad (i=1,2,3)
\end{aligned} \tag{31b}$$

where δt is a small time increment.

If the inclusion is a sphere, Eq. (29) is used to calculate its orientation at the next time step.

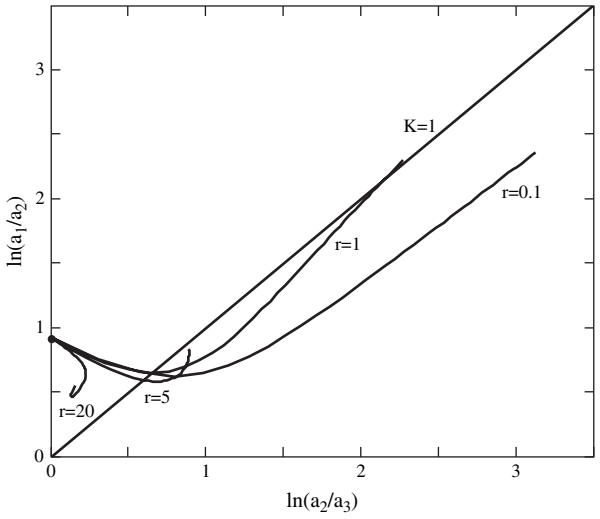

Fig. 8. The paths for the shape change of the inclusion in numerical experiment set 3 presented in a logarithm Flinn plot.

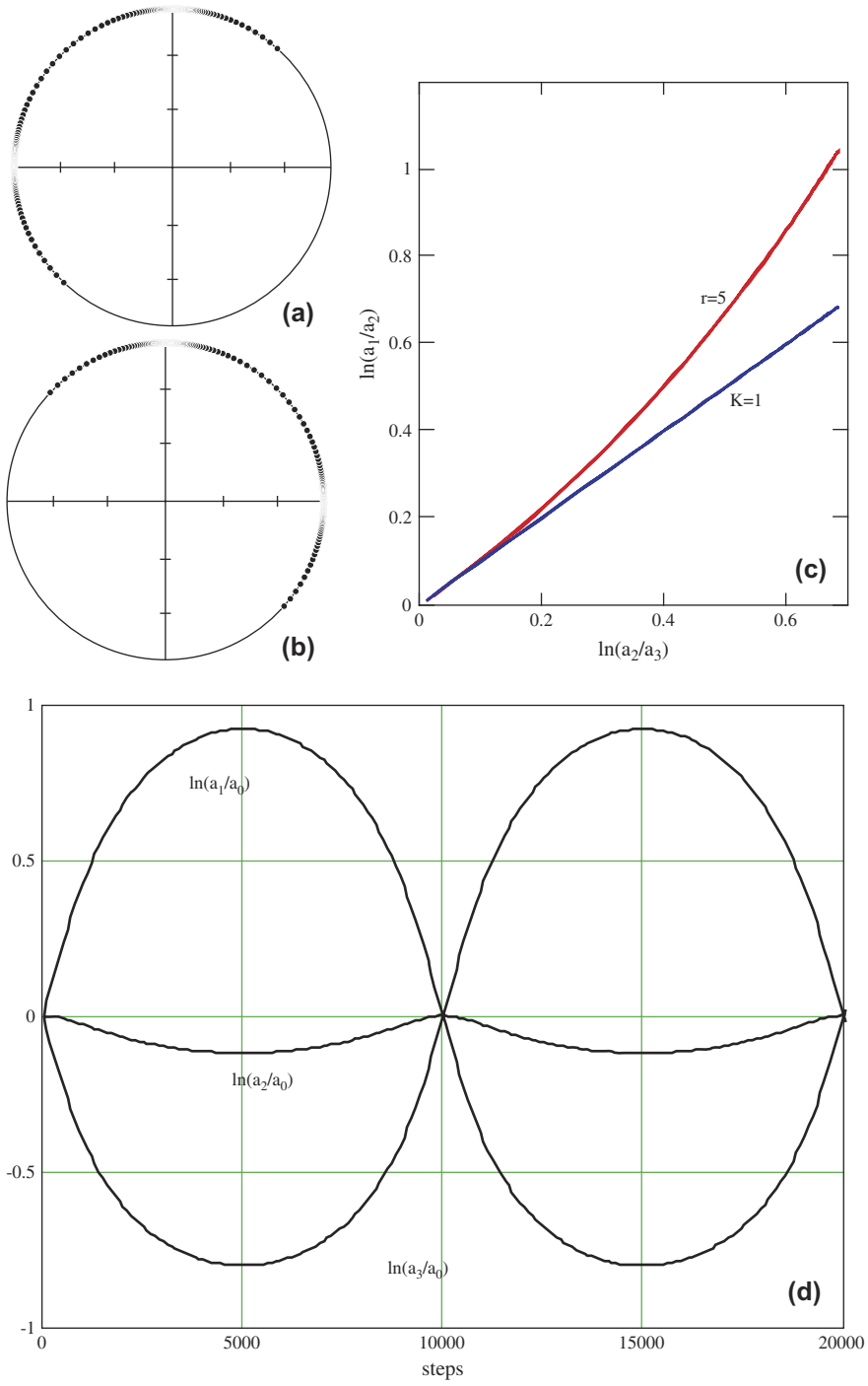

Fig. 9. (a, b) Rotation paths for an initially spherical inclusion in simple shear. The viscosity ratio is 5. The maximum (a) and minimum (b) principal axes of the inclusion lie in the vorticity-normal section. The intermediate axis (not presented) is always parallel to the vorticity vector. The maximum axis starts at 45° and the minimum axis at 135° with respect to the shear plane and it rotates with the vorticity. Every 90° of rotation, the inclusion returns to perfect spherical state. (c) The shape evolution path of the inclusion. The inclusion pulsates between sphere and the maximum strained state (c). (d) The natural strains of the three principal axes of the inclusion. The inclusion pulsates and the maximum and minimum axes swap status periodically. Although the matrix flow is of plane-strain type, there is strain parallel to the intermediate axis and the inclusion plots in the constrictional field.

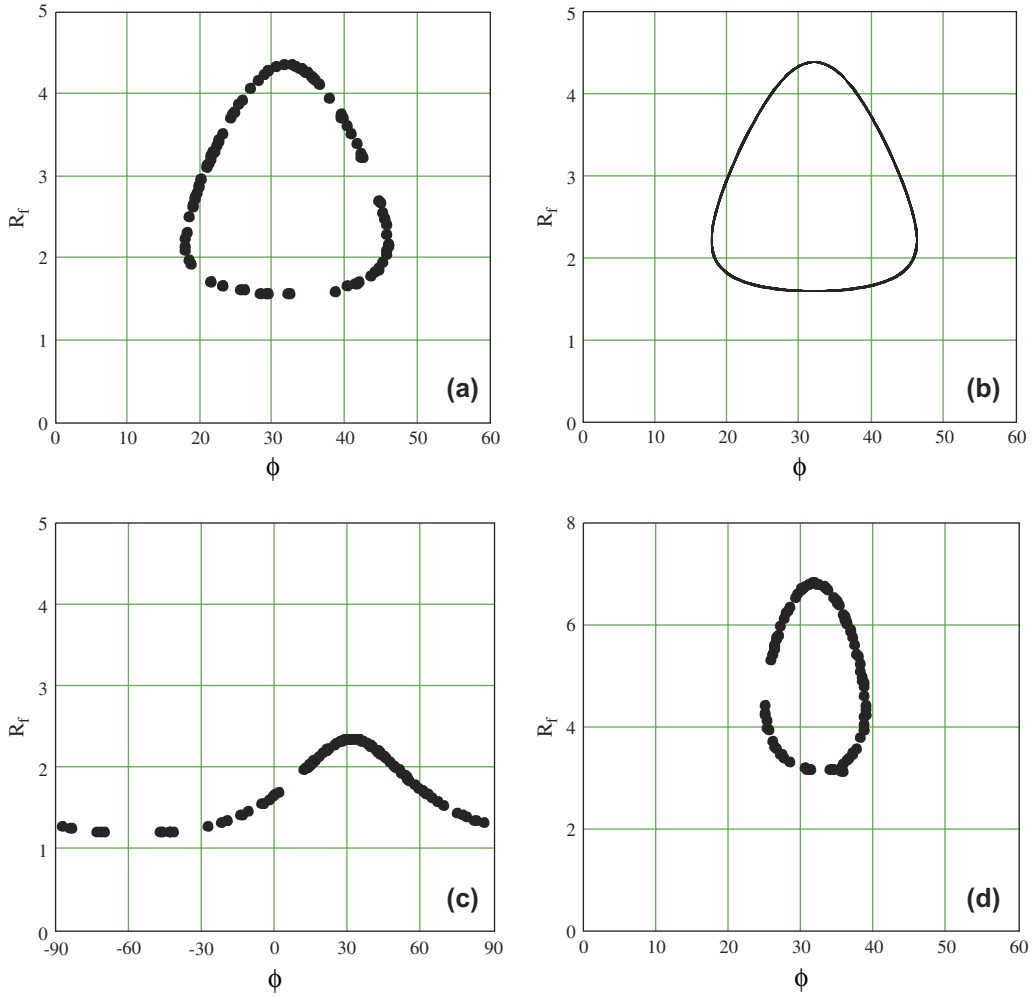

Fig. 10. R_f/φ plot on the vorticity-normal section for a population of 100 inclusions. The inclusions are very elongated clasts with axial ratio of 5:3:100. The long axis for each and every clast is parallel to the vorticity vector. The other two axes for the clasts are uniform randomly distributed on the vorticity-normal section in the initial state. The bulk flow is simple shear and the final shear strain is 1. (a) Perfectly passive clasts. The final elliptical shapes (R_f) and their long axis orientations (φ) agree perfectly with the prediction (b) based on the equations of Ramsay (1967, pp. 205–209). (c) Competent clasts (viscosity ratio of 5 for all clasts). (d) Incompetent clasts (viscosity ratio of 0.1 for all clasts).

The Runge–Kutta fourth-order approximation for Eq. (30b) leads to:

$$
\begin{aligned}
h_1 &= \delta t D^{\mathrm{E}}_{ii}(t_n) a_i(t_n) \\
h_2 &= \delta t D^{\mathrm{E}}_{ii}\left(t_n+\frac{\delta t}{2}\right)\left(a_i(t_n)+\frac{1}{2}h_1\right) \\
h_3 &= \delta t D^{\mathrm{E}}_{ii}\left(t_n+\frac{\delta t}{2}\right)\left(a_i(t_n)+\frac{1}{2}h_2\right) \\
h_4 &= \delta t D^{\mathrm{E}}_{ii}(t_n+\delta t)(a_i(t_n)+h_3) \\
a_i(t_{n+1}) &\approx a_i(t_n)+\frac{1}{6}(h_1+2h_2+2h_3+h_4) \\
&(i=1,2,3)\ \text{no summation}
\end{aligned}
\tag{32}
$$

Both $D^{\mathrm{E}}_{ii}(t_n)$ and $\mathbf{\Theta}(t_n)$ are functions of the current orientation, $\mathbf{e}'_i(t_n)$, and axial lengths, $a_i(t_n)$, of the object which can be calculated for the current state of the object. To obtain $\mathbf{\Theta}(t_n+(\delta t/2))$, $\mathbf{\Theta}(t_n+\delta t)$, $D^{\mathrm{E}}_{ii}(t_n+(\delta t/2))$, and $D^{\mathrm{E}}_{ii}(t_n+\delta t)$ for Eqs. (31) and 32, we do need to first obtain the object orientation and axial lengths at $t_n+(\delta t/2)$ and at $t_n+\delta t$. For this we use the Euler approximation $\mathbf{e}'_i(t_n+(\delta t/2)) \approx \mathbf{e}'_i(t_n)+(\delta t/2)\mathbf{\Theta}(t_n)\mathbf{e}'_i(t_n)$, $\mathbf{e}'_i(t_n+\delta t) \approx \mathbf{e}'_i(t_n)+\delta t\mathbf{\Theta}(t_n)\mathbf{e}'_i(t_n)$, $a_i(t_n+(\delta t/2)) \approx a_i(t_n)+(\delta t/2)D^{\mathrm{E}}_{ii}(t_n)a_i(t_n)$, and $a_i(t_n+\delta t) \approx a_i(t_n)+\delta t D^{\mathrm{E}}_{ii}(t_n)_i a_i(t_n)$. In the event the inclusion is a spheroid, $\mathbf{e}'^{*}_i(t_n)$ (Eq. (27)) must be used in places of $\mathbf{e}'_i(t_n)$ for these Euler approximations.

In summary, the new orientation $\mathbf{e}'_i(t_{n+1})$ and axial lengths $a_i(t_{n+1})$ of the object after a time increment δt can be obtained once $\mathbf{e}'_i(t_n)$, $a_i(t_n)$, and the viscosity contrast are known. The initial axial lengths of the object and the viscosity contrast are given. Jiang (in press) has shown how $\mathbf{e}'_i$ for the initial state can be calculated from the initial orientation of the inclusion. Therefore, Eq. (30) can be solved numerically using the iterative computation of Eqs. (31) and (32). Continuing with the computation for as many steps as

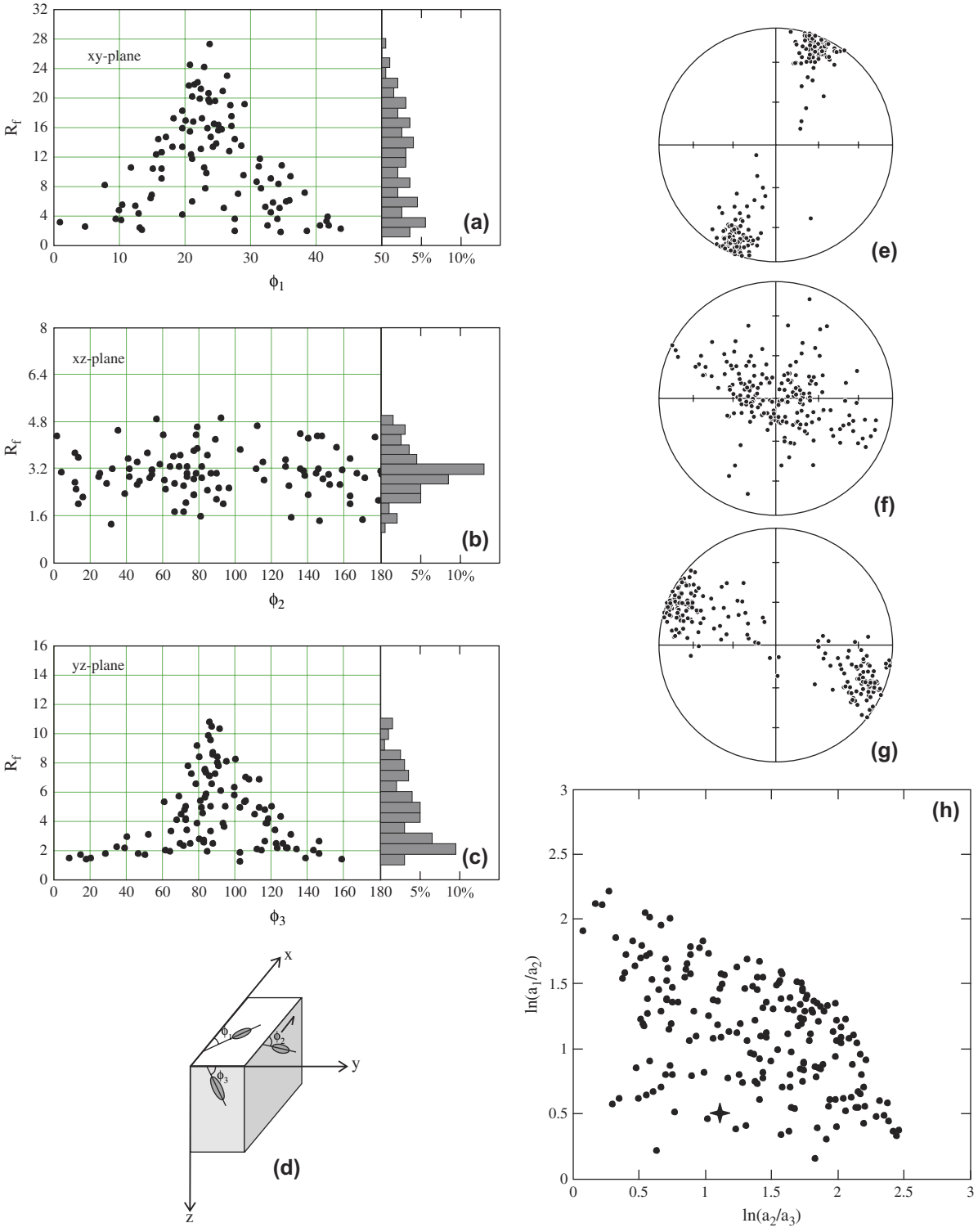

Fig. 11. R_f/φ plots (a–c) on three sections (orientation shown on (d)) at a shear strain of 2 under simple shear for a population of 200 triaxial objects (all 5:3:1 initially) that are uniformly oriented initially (orientation data generated according to the method of Jiang, in press). The histogram associated with each section shows the 2D shape distribution of the ellipses. Data of this nature can be obtained for a plane of any orientation. (e–g) Lower hemisphere equal-area projections of, respectively, the longest, intermediate, and the shortest axes at the final state. (h) Logarithm Flinn plot of all the inclusions at the final state. All inclusions were of the same shape (cross star) initially.

needed, one tracks the rotation and strain paths of the object from its initial state to its final state. The time increment δt controls the precision of the numerical calculation. The Runge–Kutta method is a very accurate method; the local errors involved in the determination of $\mathbf{e}'_i(t_{n+1})$ and $a_i(t_{n+1})$ from $\mathbf{e}'_i(t_n)$ and $a_i(t_n)$ are equivalent to the fifth order of δt (Jeffrey, 1995, p. 341). Therefore, an estimate of the error in the orientation of the object for each time step computation is then on the order of $|\boldsymbol{\omega}|(\delta t)^5$, where $|\boldsymbol{\omega}|$ is the magnitude of the instantaneous angular velocity. If we take an angular velocity of magnitude $1\ \mathrm{Ma}^{-1}$ ($\sim 3.17\times10^{-14}\ \mathrm{s}^{-1}$), using a $\delta t = 0.01$ Ma will yield an error on the order of 10^{-10} radians for each step of computation. The error in axial lengths is on the same order.

3. Mathcad® worksheets for modeling strain and rotation path of individual inclusions and preferred orientation and shape fabrics defined by a population of deformable inclusions

To determine the motion history of a deformable object is to determine the time history of the lengths of its three principal axes and their orientations. Following Jiang (in press), the orientation of a line is defined by two polar coordinate angles: the angle θ between x-axis and the projection of the line on the xy-plane, and the angle ϕ between z-axis and the line (Fig. 2a). The orientation of a triaxial ellipsoid is defined by three coordinate angles – θ_1 and ϕ_1 for the a_1-axis plus θ_2 for the second axis. In the special case of $\phi_1 = \pi/2$, the triplet (θ_1, ϕ_1, ϕ_2) is used instead, where ϕ_2 is the angle for the a_2-axis associated with the trend angle $\theta_2 = \theta_1 + 90^\circ$ (see Jiang, in press). The viscosity contrast and the initial lengths of the principal axes of the inclusion are given. From this initial state, successive states of the inclusion – the strain and rotation history of the inclusion – can be tracked for any given bulk flow.

Although Eshelby's theory, like Jeffery's, was developed for a single isolated ellipsoidal inclusion, it is applicable to a population of inclusions, if the inclusions are spaced sufficiently far apart so that their interactions are negligible. The work of Mandal et al. (2003) suggests that for pure shear if the spacing between adjacent objects is greater than twice the size of the object, they are practically non-interacting.

Mathcad® (http://www.mathsoft.com) worksheets (Supplement file) are written based on the algorithm presented above. A few examples of applying the worksheets are presented below.

4. Examples of applying the Mathcad worksheets

4.1. Strain and rotation path of a single inclusion

To model the rotation and strain path of an individual inclusion, use Worksheet 1 (Supplement). In the section of "Input Variables", input the following variables: (1) the inclusion's initial state, $\mathbf{x}_0$, which is a vector of six components, (2) the viscosity ratio, r, (3) the matrix flow velocity gradient tensor, $\mathbf{L}$, (4) the time step δt, (5) the total steps of running, *STEPS*, and (6) the number of steps of computation, *mm*, between output sets. The total actual time duration of the deformation is $STEPS\cdot\delta t$, and the time interval between successive output sets is $mm\cdot\delta t$. At the end of computation, the output is in the Excel spreadsheet format which can be plotted either within Mathcad or using other applications.

For all the following modeling experiments, the matrix flow is a simple shear defined in the geographic coordinate system (Fig. 2b). The shear plane is the vertical xz-plane, the shear direction is parallel to the x-direction, and the sense of shear is sinistral.

Numerical experiment set 1: Rotation path and shape evolution of a triaxial inclusion with initial axial ratio of 5:3:1. The complete initial state of the inclusion is specified by the sextex (170°, 45°, 30°, 5, 3, 1). Fig. 3 presents the rotation paths of a triaxial inclusion up to a matrix shear strain of 10. Fig. 3a–c are, respectively, for a_1, a_2, and a_3 axes for the case of $r = 0.1$, Fig. 3d–f for the case of $r = 1$, Fig. 3g–i for the case of $r = 5$, and Fig. 3j–l for the case of $r = 20$. Fig. 3m–o presents the rotation paths for a rigid ellipsoid with the same initial state calculated using Jeffery's theory (Jiang, in press). In the case of $r = 5$, the inclusion passes through an oblate state and the relative lengths of a_1- and a_2-axes changed during deformation. Fig. 4 presents the corresponding shape evolution histories of the triaxial inclusion in a logarithm Flinn plot. For the case of $r = 5$, $a_1 = a_2$ when the inclusion was perfectly oblate. After that $a_1 < a_2$. In Fig. 4, it can be clearly seen that the a_1- and a_2-axes were manually swapped after the inclusion passed the oblate state.

Numerical experiment set 2: Rotation path and shape evolution in simple shear of an initially oblate inclusion with axial lengths 5:5:2 and complete initial state (170°, 45°, 30°, 5, 5, 2). Fig. 5 presents the rotation paths up to a matrix shear strain of 10. Fig. 5a–c are, respectively, for a_1, a_2, and a_3 axes for the case of $r = 0.1$, Fig. 5d–f for the case of $r = 1$, Fig. 5g–i for the case of $r = 5$, and Fig. 5j–l for the case of $r = 20$. Although the specified initial orientation of the a_1-axis plunges 45° toward 170°, its orientation after an infinitesimal strain increment is widely different from the initial orientation. Fig. 6 presents the corresponding shape evolution histories of the inclusion in a logarithm Flinn plot.

Numerical experiment set 3: Rotation path and shape evolution of an initially prolate inclusion with axial ratio of 5:2:2 and complete initial state (170°, 45°, 30°, 5, 2, 2). Fig. 7 presents the rotation paths up to a matrix shear strain of 10. Fig. 7a–c are, respectively, for a_1, a_2, and a_3 axes for the case of $r = 0.1$, Fig. 7d–f for the case of $r = 1$, Fig. 7g–i for the case of $r = 5$, and Fig. 7j–l for the case of $r = 20$. Similar to the oblate situation, although the specified initial orientation of the a_2-axis trends at 30°, its orientation after an infinitesimal strain increment is widely different from the initial orientation. Fig. 8 presents the corresponding shape evolution histories of the inclusion in a logarithm Flinn plot.

Numerical experiment set 4: Rotation path and shape evolution of an initially spherical inclusion with radius of 5 in

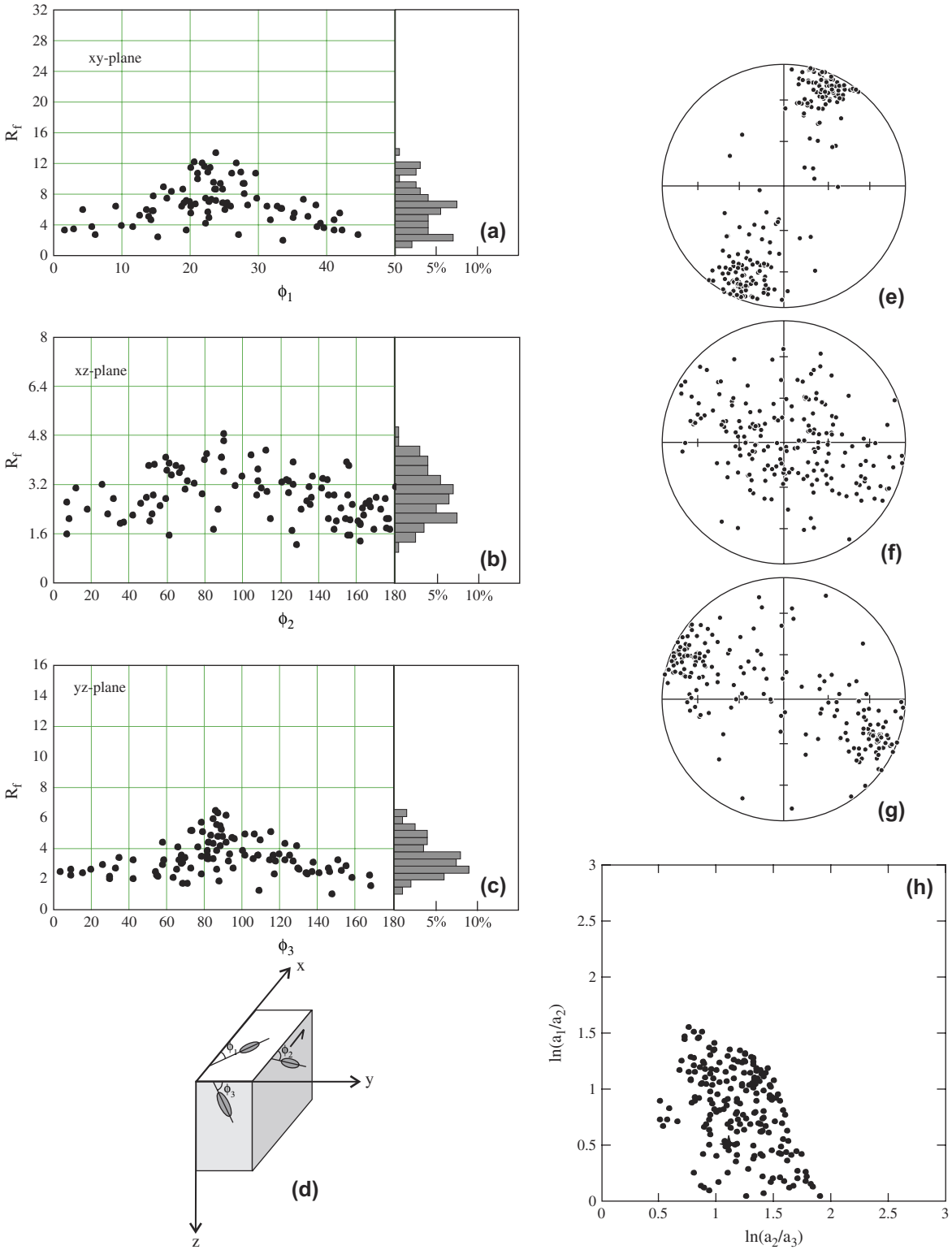

Fig. 12. Plots similar to Fig. 11 for a numerical experiment identical to that for Fig. 11 except that the viscosity ratio is 5.

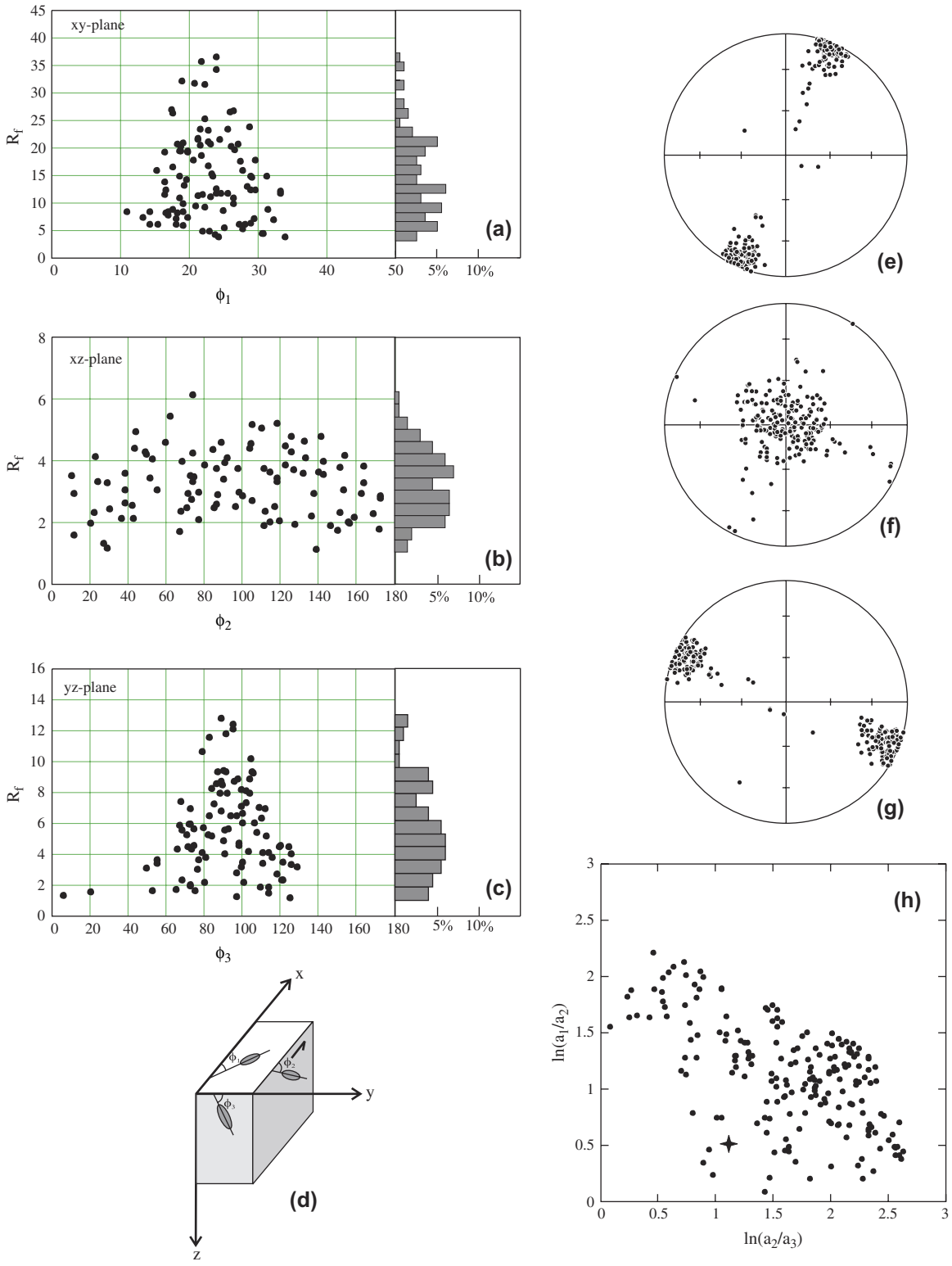

Fig. 13. Plots similar to Fig. 11 for a numerical experiment identical to that for Fig. 11 except that the viscosity ratio is 0.1.

simple shear. The viscosity ratio is 5. Fig. 9 presents the rotation paths of the two principal axes lying in the vorticity-normal section. The deformation of the inclusion pulsates. The maximum principal axis of the inclusion starts at 45° with respect to the shear plane in the vorticity-normal section and the minimum principal axis starts at 135° with respect to the shear plane. They both rotate with vorticity in the *xy*-plane (Fig. 2b, the vorticity-normal section of the flow) (Fig. 9a, b). Every 90° of rotation, the inclusion returns to perfect spherical state (Fig. 9d). The shape of the inclusion is in the constrictional strain field on the Flinn plot and there is pulsating strain along the vorticity direction even though the matrix deformation is a plane-strain simple shear.

4.2. Fabric development of a population of inclusions

To model the development of preferred orientation fabric and shape fabric defined by a population of inclusions, use Worksheet 2 (Supplement). First supply all the input variables. In addition to the flow velocity gradient tensor, **L**, the viscosity contrast, r, the time increment, δt, and the total steps of computation, STEPS, the input variables include the dataset for the initial orientations and axial lengths of all the objects and the number of objects. The initial orientations of the objects can be generated through Excel using the method described in Jiang (in press). The initial axial lengths and viscosity ratios can be defined to follow certain distributions as well. The dataset is inserted into the worksheet. If the R_f/φ data on a plane is required, one must provide the strike and dip of the plane. Once all input variables are supplied, evaluate the worksheet. At the end of computation, the output can be both in the Excel spreadsheet format and/or in diagrams. The final output will include the trend and plunge angles of the principal axes of each and every object, the axial lengths of each and every object, and the R_f/φ data on the 2D section. The following examples are all for a simple shear deformation defined in the geographic coordinate system (Fig. 2b). The shear direction is parallel to the x-axis and the sense of shear is sinistral.

Numerical experiment set 5: In this set of numerical experiments, we first compare the 2D deformation of passive elliptical objects based on equations of Ramsay (1967) and Dunnet (1969) with the modeling results. We generate a population of 100 very elongate inclusions, all with axial lengths of 5:3:100 (approaching elliptical cylinders). The long axes of all inclusions are vertical (parallel to the vorticity vector). The intermediate and short axes are uniform randomly distributed, in the initial state, on the horizontal *xy*-plane (vorticity-normal section). This dataset implies that on the horizontal plane, the elliptical shapes of all inclusions are identical, with an axial ratio of 5:3. The long axis orientations are uniform random. When the viscosity ratio is 1, the inclusions are completely passive. Subject this population of inclusions to simple shear. Fig. 10a presents the R_f/φ plot on the vorticity-normal section when the bulk shear strain is 1. The modeling result (Fig. 10a) agrees perfectly with plot (Fig. 10b) based on the equations of Ramsay (1967, pp. 205–209). Fig. 10c, d present results of numerical experiments for the same population of inclusions deformed to the same magnitude of bulk shear strain as for Fig. 10a, but with different viscosity ratios: 5 for Fig. 10c and 0.1 for Fig. 10d.

Numerical experiment set 6: Figs. 11, 12, and 13 present results of three numerical experiments with viscosity ratios, respectively, being 1, 5, and 0.1. In these experiments, a population of 200 inclusions all of the same shape (with an axial ratio of 5:3:1) are deformed in simple shear flow. The initial orientations of the inclusions are uniform randomly distributed in 3D space. Such an orientation dataset is generated according to the method of Jiang (in press). The final shear strain of the matrix is 2. Fig. 11 presents result for the case the inclusions are perfectly passive ($r = 1$). Both a strong shape fabric (Fig. 11a–c) and a preferred orientation fabric defined by the three axes of inclusions (Fig. 11e–g) are developed at this strain state. Fig. 11h shows the final inclusion shapes on a logarithm Flinn diagram. Fig. 12 presents the results of a similar experiment for competent inclusions ($r = 5$), and Fig. 13 the results of another similar experiment for incompetent inclusions ($r = 0.1$).

5. Concluding remarks

Eshelby's theory covers the entire spectrum from void behavior ($r = 0$) (cf. Schmid and Podladchikov, 2004), to weak inclusion behavior ($0 < r < 1$), to perfectly passive inclusion behavior ($r = 1$), through strong inclusion behavior ($r > 1$), to rigid inclusion behavior ($r \to \infty$). For passive inclusions, the theory is reduced to the theoretical basis for the R_f/φ analysis in structural geology (Ramsay, 1967; Dunnet, 1969). At high viscosity ratios, the theory asymptotically approaches that of Jeffery's (1922) theory. Eshelby's theory has been and will continue to be widely applied in geology and the broad field of materials science.

The numerical algorithm presented in this paper has handled all singular cases in the general solution of Eshelby's equations. The implementation of the algorithm in a fully graphic mathematics application, Mathcad® (www.mathsoft.com) allows numerical investigation based on Eshelby's theory to be as easily carried out as using a spreadsheet. Although the examples presented are all in simple shear because it is the most familiar flow type to geologists, the worksheets handle all types of three-dimensional flows with equal ease. Since the computation is completely under the control of the modeler through a fully graphic interface, it is easy for the modeler to customize the computation so that the type and format of the output data best fit the purpose of the investigation.

Acknowledgements

I thank B. Grasemann and K.F. Mulchrone for their review comments of the manuscript. Support from an NSERC

discovery grant and the University of Western Ontario Academic Development Funds is acknowledged.

Appendix A. Supplementary data

Supplementary data associated with this article can be found, in the online version, at doi:10.1016/j.jsg.2006.09.009.

References

Arbaret, L., Mancktelow, N.S., Burg, J.-P., 2001. Effect of shape and orientation on rigid particle rotation and matrix deformation in simple shear flow. Journal of Structural Geology 23, 113–125.

Başar, Y., Weichert, D., 2000. Nonlinear Continuum Mechanics of Solids. Springer, Berlin.

Benedikt, B., Lewis, M., Rangaswamy, P., 2006. On elastic interactions between spherical inclusions by the equivalent inclusion method. Computational Materials Science 37, 380–392.

Bilby, B.A., Eshelby, J.D., Kundu, A.K., 1975. The change of shape of a viscous ellipsoidal region embedded in a slowly deforming matrix having a different viscosity. Tectonophysics 28, 265–274.

Bilby, B.A., Kolbuszewski, M.L., 1977. The finite deformation of an inhomogeneity in two-dimensional slow viscous incompressible flow. Proceedings of the Royal Society of London A355, 335–353.

Bretherton, F.P., 1962. The motion of rigid particles in shear flow at low Reynolds number. Journal of Fluid Mechanics 14, 284–301.

ten Brink, C.E., 1996. Development of Porphyroclast Geometries during Non-Coaxial Flow. In: Geologica Ultraiectina, vol. 142. 163.

Ceriani, S., Mancktelow, N.S., Pennacchioni, G., 2003. Analogue modelling of the influence of shape and particle/matrix interface lubrication on the rotational behaviour of rigid particles in simple shear. Journal of Structural Geology 25, 2005–2021.

Dunnet, D., 1969. A technique of finite strain analysis using elliptical particles. Tectonophysics 7, 117–136.

Eirich, F., Mark, H., 1937. Ueber Lösungsmittelbindung durch Immobilisierung. Papierfabrikant 27, 251–258.

Eshelby, J.D., 1957. The determination of the elastic field of an ellipsoidal inclusion, and related problems. Proceedings of the Royal Society of London A241, 376–396.

Eshelby, J.D., 1959. The elastic field outside an ellipsoidal inclusion. Proceedings of the Royal society of London A252, 561–569.

Fletcher, R.C., 2004. Anisotropic viscosity of a dispersion of aligned elliptical cylindrical clasts in viscous matrix. Journal of Structural Geology 26, 1977–1987.

Freeman, B., 1985. The motion of rigid ellipsoidal particles in slow flows. Tectonophysics 113, 163–183.

Freeman, B., 1987. The behavior of deformable ellipsoidal particles in three-dimensional slow flows: implications for geological strain analysis. Tectonophysics 132, 297–309.

Gay, N.C., 1966. Orientation of mineral lineation along the flow direction in rocks: a discussion. Tectonophysics 3, 559–564.

Gay, N.C., 1968a. The motion of rigid particles embedded in a viscous fluid during pure shear deformation of the fluid. Tectonophysics 5, 81–88.

Gay, N.C., 1968b. Pure shear and simple shear deformation of inhomogeneous viscous fluids. 1. Theory. Tectonophysics 5, 211–234.

Ghosh, S.K., Ramberg, H., 1976. Reorientation of inclusions by combination of pure shear and simple shear. Tectonophysics 34, 1–70.

Goddard, J.D., Miller, C., 1967. Nonlinear effects in the rheology of dilute suspensions. Journal of Fluid Mechanics 28, 657–673.

Goldsmith, H.L., Mason, S.G., 1967. The microrheology of dispersions. In: Eirich, F.R. (Ed.), Rheology, Theory and Applications, vol. 4, pp. 85–250.

Ildefonse, B., Launeau, P., Bouchez, J.-L., Fernandez, A., 1992a. Effect of mechanical interactions on the development of shape preferred orientations: a two-dimensional experimental approach. Journal of Structural Geology 14, 73–83.

Ildefonse, B., Mancktelow, N.S., 1993. Deformation around rigid particle: influence of slip at the particle/matrix interface. Tectonophysics 221, 345–359.

Ildefonse, B., Sokoutis, D., Mancktelow, N.S., 1992b. Mechanical interactions between rigid particles in a deforming ductile matrix. Analogue experiments in simple shear flow. Journal of Structural Geology 14, 1253–1266.

Jeffery, G.B., 1922. The motion of ellipsoidal particles immersed in a viscous fluid. Proceedings of the Royal Society of London A102, 161–179.

Jeffrey, A., 1995. Handbook of Mathematical Formulas and Integrals. Academic Press, New York.

Jezek, J., Melka, R., Schulmann, K., Venera, Z., 1994. The behaviour of rigid triaxial ellipsoidal particles in viscous flows – modeling of fabric evolution in a multiparticle system. Tectonophysics 229, 165–180.

Jezek, J., Schulmann, K., Segeth, K., 1996. Fabric evolution of rigid inclusions during mixed coaxial and simple shear flows. Tectonophysics 257, 203–221.

Jiang, D., 1999. Vorticity decomposition and its application to sectional flow characterization. Tectonophysics 301, 243–259.

Jiang, D. Numerical modeling of the motion of rigid ellipsoidal objects in slow viscous flows: a new approach. Journal of Structural Geology, in press.

Launeau, P., Cruden, A.R., 1998. Magmatic fabric acquisition mechanisms in a syenite: results of a combined anisotropy of magnetic susceptibility and image analysis study. Journal of Geophysical Research 103, 5067–5089.

Lee, K.Y., Paul, D.R., 2005. A model for composites containing three-dimensional ellipsoidal inclusions. Polymer 46, 9064–9080.

Lisle, R.J., 1985. Geological Strain Analysis: A Manual for the R_f/ϕ Technique. Pergamon Press, Oxford.

Lister, G.S., 1982. A vorticity equation for lattice reorientation during plastic deformation. Tectonophysics 82, 351–366.

Lister, G.S., Williams, P.F., 1983. The partitioning of deformation in flowing rock masses. Tectonophysics 92, 1–33.

Liu, X., Hu, G., 2004. Inclusion problem of microstretch continuum. International Journal of Engineering Science 42, 849–860.

Ma, H., Liu, X., Hu, G., 2006. Overall elastoplastic property for micropolar composites with randomly oriented ellipsoidal inclusions. Computational Materials Science 37, 582–592.

Mancktelow, N.S., Arbaret, L., Pennacchioni, G., 2002. Experimental observations on the effect of interface slip on rotation and stabilisation of rigid particles in simple shear and a comparison with natural mylonites. Journal of Structural Geology 24, 567–585.

Mandal, N., Samanta, S.K., Bhattacharyya, G., Chakraborty, C., 2003. Deformation of ductile inclusions in a multiple inclusion system in pure shear. Journal of Structural Geology 25 (9), 1359–1370.

Mandal, N., Kumar Samanta, S., Bhattacharyya, G., Chakraborty, C., 2005a. Rotation behaviour of rigid inclusions in multiple association: insights from experimental and theoretical models. Journal of Structural Geology 27, 679–692.

Mandal, N., Misra, S., Samanta, S.K., 2005b. Rotation of single rigid inclusions embedded in an anisotropic matrix: a theoretical study. Journal of Structural Geology 27, 731–743.

March, A., 1932. Mathematische Theorie der Regelung nach der Korngestalt bei affiner deformation. Zeitschrift für Kristallographie 81, 285–297.

Marques, F.O., Bose, S., 2004. Influence of a permanent low-friction boundary on rotation and flow in rigid inclusion/viscous matrix systems from an analogue perspective. Tectonophysics 382, 229–245.

Marques, F.O., Coelho, S., 2001. Rotation of rigid elliptical cylinders in viscous simple shear flow: analogue experiments. Journal of Structural Geology 23, 609–617.

Masuda, T., Michibayashi, K., Ohta, H., 1995. Shape preferred orientation of rigid particles in a viscous matrix: reevaluation to determine kinematic parameters of ductile deformation. Journal of Structural Geology 17, 115–129.

Mura, T., 1987. Micromechanics of Defects in Solids. Martinus Nijhoff Publishers, Dordrecht/Boston/Lancaster.

Passchier, C.W., 1987. Stable positions of rigid objects in non-coaxial flow – a study in vorticity analysis. Journal of Structural Geology 9, 679–690.

Passchier, C.W., Simpson, C., 1986. Porphyroclast systems as kinematic indicators. Journal of Structural Geology 8, 831–843.

Ramsay, J.G., 1967. Folding and Fracturing of Rocks. McGraw-Hill Book Company, New York.

Reed, J.L., Tryggvason, E., 1974. Preferred orientation of rigid particles in a viscous matrix deformed by pure shear and simple shear. Tectonophysics 24, 85–98.

Robertson, C.R., Acrivos, A., 1970. Low Reynolds number shear flow past a rotating circular cylinder. Part 1: Momentum transfer. Journal of Fluid Mechanics 40, 685–704.

Schmid, D.W., Podladchikov, Y.Y., 2004. Are isolated stable rigid clasts in shear zones equivalent to voids? Tectonophysics 384, 233–242.

Schmid, D.W., Podladchikov, Y.Y., 2005. Mantled porphyroclast gauges. Journal of Structural Geology 27, 571–585.

Spencer, A.J.M., 1980. Continuum Mechanics. Longman, London.

Taylor, G.I., 1923. The motion of ellipsoidal particles immersed in a viscous fluid. Proceedings of the Royal Society of London A103, 58–61.

Treagus, S.H., 2002. Modelling the bulk viscosity of two-phase mixtures in terms of clast shape. Journal of Structural Geology 24, 57–76.

Treagus, S.H., Treagus, J.E., 2001. Effects of object ellipticity on strain, and implications for clast–matrix rocks. Journal of Structural Geology 23, 601–608.

Treagus, S.H., Treagus, J.E., 2002. Studies of strain and rheology of conglomerates. Journal of Structural Geology 24, 1541–1567.

Trevelyan, B.J., Mason, S.G., 1951. Particle motions in sheared suspensions. I. Rotations. Journal of Colloid Science 6, 354–367.

Truesdell, C.A., Topin, R.A., 1960. The classic field theory. In: Flügge, S. (Ed.), Encyclopedia of Physics. Principles of Classic Mechanics and Field Theory, vol. III. Springer-Verlag, Berlin, pp. 226–793.

Tullis, T.E., 1976. Experiments on the origin of slaty cleavage and schistosity. Geological Society of America Bulletin 87, 745–753.

Willis, D.G., 1977. A kinematic model of preferred orientation. Geological Society of America Bulletin 88, 883–894.